arXiv:1408.3440v1 [physics.atom-ph] 14 Aug 2014

,

Valence-shell single photoionization of Chlorine-like K^{2+} ions: Experiment and Theory

G. A. Alna'Washi,* M. Lu, M. Habibi, D. Esteves-Macaluso,† J. C. Wang, and R. A. Phaneuf
Department of Physics, University of Nevada, Reno, NV 89557-0220

A. L. D. Kilcoyne
Advanced Light Source, Lawrence Berkeley National Laboratory, 1 Cyclotron Road, Berkeley, CA 94720

C. Cisneros
Instituto de Ciencias Físicas, Universidad Nacional Autónoma de México, Apartado Postal 48-3, Cuernavaca 62210, Morelos, México.

B. M. McLaughlin‡
Institute for Theoretical Atomic and Molecular Physics, Harvard Smithsonian Center for Astrophysics, 60 Garden Street, MS-14, Cambridge, MA 02138

(Dated: August 18, 2014)

The absolute single photoionization cross-section was measured for Cl-like K^{2+} over the photon energy range from 44.2 - 69.7 eV at a constant energy resolution of 0.045 eV. The experiments were performed by merging an ion beam with a beam of synchrotron radiation from an undulator. The ground-state ionization threshold was measured at 0.004 eV energy resolution to be 45.717 ± 0.030 eV. The measurements are rich in resonance structure due to multiple Rydberg series of transitions to autoionizing states. These series are assigned spectroscopically using the quantum defect method, guided by pseudo-relativistic Hartree-Fock calculations for the energies and oscillator strengths of transitions to autoionizing states. The experimental results, which include significant contributions from K^{2+} ions initially in metastable states, are in satisfactory agreement with a linear superposition of semi-relativistic R-matrix calculations of photoionization cross sections from these initial states.

PACS numbers: 32.80.Fb 32.80.Zb 32.80.Ee

I. INTRODUCTION

Studies of photoionization of atomic ions lead to a fundamental understanding of atomic interactions occurring in the earth's atmosphere [1] and in high temperature environments such as stars, nebulae [2] and controlled thermonuclear fusion reactors [3]. Experiments on photoionization of atomic and molecular ions have become possible by utilizing the high photon flux of third-generation synchrotron radiation sources and the photon-ion merged-beams technique [4–6], facilitating measurements at an unprecedented level of refinement and precision. Photoionization cross sections of potassium ions have many applications in astrophysics. Various lines of K^{2+} (K III) and K^{3+} (K IV) ions have been detected in the planetary nebula NGC 7027 by the infrared Space Observatory Short Wavelength Spectrometer (SWS) [7]. An analysis using a simplified photoionization model with CLOUDY [8, 9] produced acceptable results when modeling the NGC 6302 neon line intensities from various ionization stages. The model predicts a K VII line to be the brightest of the K III to K VII series of ionic lines. The measured upper limits for the lower-excitation [K] lines in the SWS spectrum of NGC 6302 are consistent with intensities predicted by the model. However there is always room for improvement and the need for more accurate atomic data is essential for these types of predictions. Furthermore, K III and K VI lines are also seen in the ultraviolet and visible spectra of the symbiotic nova RR Telescopii [10, 11] and in the coronal line region of planetary nebulae NGC 6302 and NGC 6537 [12].

The photoionization process provides a highly selective probe of the internal electronic structure and dynamics of atoms, molecules and their ions. Systematic studies along isoelectronic sequences are useful in predicting unknown spectra for other members of the sequence. Strong electron-electron interactions introduce complexity to the electronic structure of the chlorine isoelectronic sequence. Apart from the work of our group, only limited experimental measurements have been carried out of photoionization cross sections for this isoelectronic sequence. We note that preliminary studies of $2p$ photoabsorption in Cl, Ar^+, K^{2+}, and Ca^{3+} ions were made by Martins et al. [13] but full details were not published. This work

* alnawashi@hu.edu.jo; Present address: Department of Physics, The Hashemite University, Zarqa 13115, Jordan
† david.macaluso@umontana.edu; Present address: Department of Physics and Astronomy, University of Montana, Missoula, Montana 59812, USA
‡ b.mclaughlin@qub.ac.uk; Present address: Centre for Theoretical Atomic, Molecular and Optical Physics (CTAMOP), School of Mathematics and Physics, The David Bates Building, 7 College Park, Queen's University of Belfast, Belfast BT7 1NN, United Kingdom

was recently extended in a detailed study of inner-shell photoionization of Cl by Stolte and co-workers [14], who measured relative partial ionization cross sections following photoexcitation of atomic chlorine near the Cl $2p$ and Cl $1s$ ionization thresholds. Accompanying Breit-Pauli R-matrix theoretical calculations performed in the region of the $2p$ thresholds showed suitable agreement with experiment.

Photoionization of atomic chlorine in the valence region was studied experimentally by several groups using photoelectron spectroscopy [15–18]. Alna'Washi and co-workers performed absolute cross-section measurements for the Ca^{3+} ion using the photon-ion merged-beams method that were in satisfactory agreement with R-matrix calculations performed in intermediate coupling [19]. Similarly, absolute photoionization cross-section measurements for Ar^+ ions by Covington and co-workers [20, 21] using the merged-beams technique were also in satisfactory agreement with theory. In that study,17 Rydberg series due to $3p \rightarrow ns$ and $3p \rightarrow nd$ converging to the $^1D_2$ and $^1S_0$ states of Ar^{2+} were assigned [21]. We note that the $3p$ photoionization cross-section of Cl-like Potassium (K^{2+}) has been calculated previously using the R-matrix theoretical approach in LS-coupling [22, 23], where the presence of the $3s^23p^4(^1D_2)nd$ and $3s^23p^4(^1S_0)nd$ Rydberg series were clearly illustrated.

Photoionization of atomic chlorine has been extensively studied theoretically during the last few decades using a variety of approximations. These include R-matrix and K-matrix calculations carried out by several groups [24–27], the configuration-interaction method [28], many-body theory [29], open-shell transition-matrix [30], and an effective single-particle potential [31].

This paper completes an investigation at the Advanced Light Source of photoionization of ions of the Cl isoelectronic sequence. The absolute photoionization cross-section was measured for K^{2+} ions in the energy range 44.2 – 69.7 eV. Resonances observed in the photoionization cross section are assigned spectroscopically using quantum defect theory (QDT) guided by pseudo relativistic Hartree-Fock calculations of energies and oscillator strengths of autoionizing transitions (performed using the Cowan atomic structure code). The measurements are compared directly with new R-matrix [23] theoretical results obtained in intermediate coupling using the Breit-Pauli approximation.

II. EXPERIMENT

Absolute photoionization cross sections were measured using the merged-beams technique on the ion-photon-beam (IPB) end station on undulator beam line 10.0.1.2 of the Advanced Light Source at Lawrence Berkeley National Laboratory. A detailed description of the measurement technique was reported by Covington et al. [32] and only a brief description is presented here. Atomic potassium was thermally evaporated into the discharge of a 10-GHz permanent-magnet electron-cyclotron-resonance ion-source. Ions were extracted and accelerated by a potential difference of +6 kV, focused and collimated by a series of cylindrical einzel lenses and slits and magnetically analyzed according to their momentum-per-charge ratio. A beam of $^{39}K^{2+}$ ions was selected, collimated and directed to a 90° electrostatic deflector, which merged it onto the axis of the highly collimated photon beam. The latter was produced by an undulator and energy selected by a grazing-incidence spherical-grating monochromator. A cylindrical einzel lens focused the ion beam at the center of the interaction region of length 29.4 cm. For absolute measurements, an electrical potential of +2 kV was applied to energy-label K^{3+} product ions produced therein. Two-dimensional spatial profiles of the merged ion and photon beams were measured by three translating-slit scanners at the beginning, middle and end points of the interaction region. Product K^{3+} ions were separated from the primary K^{2+} ion beam by a 45° demerger magnet. The primary beam was collected in an extended Faraday cup, while a spherical 90° electrostatic deflector directed the product ions onto a stainless-steel plate biased at -550 V, from which secondary electrons were accelerated to a single-particle detector. The photoion yield was measured as the photon energy was stepped over the range 44.20 - 69.70 eV. Absolute photoionization cross-section measurements were performed at a number of discrete photon energies where no resonant features were present in the photoion-yield spectra.

The absolute cross-section measurements were used to place the photoion-yield on an absolute cross-section scale. The total absolute uncertainty of the photoionization cross-section measurements in this experiment is estimated to be ± 20%. The monochromator settings for the experiment with K^{2+} ions was calibrated using the IPB end-station by re-measuring the $^2D^o_{3/2}$, $^2D^o_{5/2}$, $^2P^o_{1/2}$, and $^2P^o_{3/2}$ photoionization thresholds of Kr^{3+}, for which the energies 48.79 ± 0.02 eV, 48.59 ± 0.01 eV, 46.91 ± 0.02 eV, and 46.62 ± 0.02 eV, respectively, were determined in a previous experiment [33]. The resulting uncertainty in the photon energy scale for the present K^{2+} measurements is conservatively estimated to be ± 0.030 eV.

III. THEORY

A. R-matrix calculations

For comparison with the high-resolution measurements, state-of-the-art theoretical methods using highly correlated wave functions with the inclusion of relativistic effects are required, since fine-structure effects are resolved in the experiments. R-matrix [23, 34] calculations of the photoionization cross-sections for the K^{2+} ion were performed in intermediate coupling using an efficient parallel version of the R-matrix codes [35] within the confines of a semi-relativistic Breit-Pauli approxima-

tion [23, 34]. For the photoionization calculations on this system 30 $LS\Pi$ states (58 $J\Pi$ states) were included in the close-coupling expansion arising from the following n=3 and 4 states of the residual K^{3+} ion core, namely, $1s^22s^22p^63s^23p^4[^3P,^1D,^1S]$, $1s^22s^22p^63s3p^5[^{1,3}P^o]$, $1s^22s^22p^63s^23p^3(^4S^o,^2D^o,^2P^o)3d[^{1,3,5}L^o, L = 0, 1, 2, 3]$, $1s^22s^22p^63s^23p^3(^4S^o,^2D^o,^2P^o)4s[^{1,3}P^o,^{1,3}D^o,^{3,5}S^o]$ and $1s^22s^22p^63p^6[^1S]$. The orbital basis set employed for the residual K^{3+} product ion was limited to n=4 in constructing the multi-reference-configuration-interaction wave functions used in our work. The Breit-Pauli approximation was used to calculate the energies of the 58 J^π levels of the K^{3+} residual ion arising from the above 30 $LS\Pi$ states and all the subsequent K^{2+} photoionization cross-sections. A minor shift (less than 0.5 %) of the theoretical energy levels for the K^{3+} residual ion was made in order to be in agreement with relativistic Hartree-Fock calculations [36] that are within 0.5 % of the tabulated values [37–39].

Photoionization cross-sections were calculated for the $3s^23p^5(^2P^o_{3/2})$ ground state and all the following metastable states $3s^23p^5(^2P^o_{1/2})$, $3s^23p^43d(^4D_{7/2,5/2,3/2})$, $3s^23p^43d(^4F_{9/2,7/2,5/2})$, $3s^23p^43d(^4P_{5/2,3/2,1/2})$, $3s^23p^43d(^2F_{7/2,5/2})$, $3s^23p^43d(^2G_{9/2,7/2})$ and $3s^23p^44s(^4P_{5/2,3/2,1/2})$ of the K^{2+} ion in intermediate coupling. The cross-section calculations for photoionization from metastable states provide insight into the initial-state distribution of the K^{2+} primary ion beam. Detailed structure calculations by Hibbert and co-workers [40] indicated these states lie between the $3s^23p^5(^2P^o_{3/2})$ ground state threshold and the $3s^23p^44s(^4P_{5/2,3/2,1/2})$ excited states of the K^{2+} ion.

The scattering wave functions were generated by allowing double-electron promotions out of the n=3 shell of the $3s^23p^5$ base configuration into the orbital set employed. Scattering calculations were performed with twenty continuum basis functions and a boundary radius of 14.537 Bohr radii. In the case of the $3s^23p^5(^2P^o_{3/2})$ initial ground state, the dipole selection rule requires the dipole transition matrices, $3/2^o \rightarrow 1/2^e, 3/2^e, 5/2^e$, to be calculated.

For the ground and metastable states considered, the list of dipole matrices for the various transitions are tabulated in Table I together with their ionization potentials. The percentage difference compared with the available NIST tabulated values is included to try and gauge the accuracy of the present Breit-Pauli results. In Table I the calculated ionization potentials (using the closed-channel semi-relativistic Breit-Pauli R-matrix approximation) is seen to differ from the NIST tabulated values by a few percent for most of the levels and about 8% for the higher lying excited states.

We note in the absence of available NIST tabulated values (as is the case for many of the K III levels shown here) the present Breit-Pauli results provides an estimate, particularly for the higher excited states. As can be seen from Table I, the finite basis set employed and the limited electron correlation included in the collision model illustrates the difficulty of representing the energies of these excited states accurately. This is evident from the higher lying excited metastable levels, with particularly the $3s^23p^43d'\,^2D_{5/2}$ and $3s^23p^44s\,^4P_{5/2}$ level splitting deviating by approximately 8% from the NIST tabulations. It is not the remit of this paper to provide definitive values for the excited state ionization potentials within the present limited approximation. Rather, the focus and aim of the present work is to try and provide an estimate and assess the contribution of resonance features in the photoionization cross sections from all the excited metastable levels considered here. Only extensive multi-configuration interaction atomic structure calculations (that includes fully relativistic effects), using progressively larger basis sets and configuration interaction (CI) expansions can address convergence to the definitive values for the ionization potentials and truly assess the accuracy of the present Bret-Pauli work.

Fully relativistic structure calculations (shown in Table I) for the K^{2+} (K III) ion were carried out using the Grant code GRASP [41–43] with the $3s^23p^5$, $3s3p^6$, $3s^23p^43d$ and $3s^23p^4n\ell$ (n= 4, 5 with $\ell = s$, p, d and f) configurations (205 levels), We use these calculations to try and assess the accuracy of fine-structure excitation threshold levels obtained from the closed-channel Breit-Pauli R-matrix results. As shown in Table I, the fully relativistic structure calculations using the GRASP code (with this larger basis set and CI expansion) for these same levels give much better agreement with the tabulated NIST values. The agreement is better than 4.6% with many cases at the 2% level. Extending the basis set and CI expansions further would yield better agreement with the NIST values but be prohibitive to include in a collision model. The results from these relativistic structure calculations performed with the GRASP code [41–43] shown in Table I are seen to provide a more accurate representation of the excited state metastable threshold energies and the j-level splittings in the absence of experiment. We note for the ground state ionization threshold the GRASP calculations are in excellent agreement with the NIST value.

The Hamiltonian matrices for all the $1/2^o$, $3/2^o$, $5/2^o$, $7/2^o$, $9/2^o$, $11/2^o$, $9/2^e$, $7/2^e$, $5/2^e$, $3/2^e$, and $1/2^e$ symmetries were then calculated, where the entire range of LS matrices that contribute to these J^π symmetries. For the initial $^2P^o_{3/2}$ ground state, the $^2P^o_{1/2}$ and all the metastable states listed in Table I, the electron-ion collision problem was solved (in the resonance region below and between all the thresholds) using a suitably fine energy mesh of $5\text{x}10^{-8}$ Rydbergs (0.68 μeV). These scattering calculations allowed complete resolution of the detailed resonance structure found in the appropriate photoionization cross sections for this ion. Radiation damping was also included in our scattering calculations. The theoretical cross sections were convoluted with a Gaussian distribution having a profile of the same full-width at half maximum (FWHM) as that of experiment (45 meV) which enabled a direct comparison to be made with the

TABLE I. Dipole transitions and ionization potentials (eV) for the ground and excited metastable states of K^{2+} (K III) considered in the present R-matrix calculations. Photoionization cross-section calculations were not carried out from the levels associated with the excited $3s3p^6\ ^2S_{1/2}$, $3s^23p^4(^1D)3d'\ ^2P_{3/2,1/2}$ and $3s^23p^4(^1D)3d'\ ^2D_{5/2,3/2}$ states as they are dipole allowed to the $3s^23p^5\ ^2P^\circ_{3/2,1/2}$ lower levels. The ionization thresholds are given in eV for the K^{2+} (K III) ion. NIST tabulated values are included for comparison purposes as are detailed atomic structure calculations using the GRASP code. The percentage differences Δ_1 (%) and Δ_2 (%) with the NIST values (where available) are respectively the Dirac and Breit-Pauli approximations.

Configuration	Term	GRASP[a] (eV)	NIST (eV)	R-matrix[b] (eV)	ΔE[c] (eV)	Δ_1^e (%)	Δ_2^f (%)	J^π	Label	$J^\pi \rightarrow J'^{\pi'}$ transitions
$3s^23p^5$	$^2P^o$	45.8030	45.8031	44.9229	-0.0001	-0.0	-1.9	$3/2^o$	–	$3/2^o \rightarrow 1/2^e, 3/2^e, 5/2^e$
		45.8030	45.717[‡]	44.9229	+0.0086	-0.2	-1.8	$3/2^o$		
		44.4039[d]	–	–	–	–	–	$3/2^o$		
$3s^23p^5$	$^2P^o$	45.5226	45.5346	44.6706	-0.0120	-0.7	-1.9	$1/2^o$	–	$1/2^o \rightarrow 1/2^e, 3/2^e$
$3s3p^6$	^2S	28.3728	29.6095	28.2623	-1.2367	-4.4	-4.6	$1/2^e$	First[†]	
$3s^23p^43d$	^4D	25.6736	–	23.4033	–	–	–	$7/2^e$	First	$7/2^e \rightarrow 5/2^o, 7/2^o, 9/2^o$
		25.6475	–	23.3838	–	–	–	$5/2^e$	First	$5/2^e \rightarrow 3/2^o, 5/2^o, 7/2^o$
		25.6215	–	23.3603	–	–	–	$3/2^e$	First	$3/2^e \rightarrow 1/2^o, 3/2^o, 5/2^o$
$3s^23p^43d'$	^2P	23.5743	22.8318	23.2502	+0.7425	+3.2	+1.8	$3/2^e$	Second[†]	
		23.1555	23.0051	23.3444	+0.1504	+0.6	+1.5	$1/2^e$	Second[†]	
$3s^23p^43d$	^4F	23.7927	–	21.4413	–	–	–	$9/2^e$	First	$9/2^e \rightarrow 11/2^o, 9/2^o, 7/2^o$
		23.6939	–	21,3556	–	–	–	$7/2^e$	Second	$7/2^e \rightarrow 5/2^o, 7/2^o, 9/2^o$
		23.6222	–	21.2927	–	–	–	$5/2^e$	Second	$5/2^e \rightarrow 3/2^o, 5/2^o, 7/2^o$
$3s^23p^43d$	^4P	22.5825	–	20.5340	–	–	–	$5/2^e$	Third	$5/2^e \rightarrow 3/2^o, 5/2^o, 7/2^o$
		22.6553	–	21.2283	–	–	–	$3/2^e$	Third	$3/2^e \rightarrow 1/2^o, 3/2^o, 5/2^o$
		22.7135	–	21.3949	–	–	–	$1/2^e$	Third	$1/2^e \rightarrow 1/2^o, 3/2^o$
$3s^23p^43d'$	^2D	22.1913	21.9880	20.1363	+0.2033	+0.9	-8.4	$5/2^e$	Fourth[†]	
		22.3457	22.1324	20.6083	+0.2133	+1.0	-6.9	$3/2^e$	Fourth[†]	
$3s^23p^43d$	^2F	22.0955	–	20.0613	–	–	–	$7/2^e$	Third	$7/2^e \rightarrow 5/2^o, 7/2^o, 9/2^o$
		21.8695	20.8618	19.8713	+1.0077	+4.6	-4.8	$5/2^e$	Fifth	$5/2^e \rightarrow 3/2^o, 5/2^o, 7/2^o$
$3s^23p^43d$	^2G	21.6998	–	19.3902	–	–	–	$9/2^e$	Second	$9/2^e \rightarrow 11/2^o, 9/2^o, 7/2^o$
		21.6867	–	19.3972	–	–	–	$7/2^e$	Fourth	$7/2^e \rightarrow 5/2^o, 7/2^o, 9/2^o$
$3s^23p^44s$	^4P	20.4312	20.0861	18.3658	+0.3451	+1.7	-8.6	$5/2^e$	Sixth	$5/2^e \rightarrow 3/2^o, 5/2^o, 7/2^o$
		20.2617	19.9291	20.2696	+0.3326	+1.6	+1.7	$3/2^e$	Fifth	$3/2^e \rightarrow 1/2^o, 3/2^o, 5/2^o$
		20.1595	19.8332	20.6599	+0.3263	+1.6	+4.2	$1/2^e$	Fourth	$1/2^e \rightarrow 1/2^o, 3/2^o$

[a]GRASP, $3s^23p^5$, $3s3p^6$, $3s^23p^43d$ and $3s^23p^4n\ell$ (n= 4, 5 with $\ell = s$, p, d and f) configurations used in the calculations.
[b]Breit-Pauli R-matrix, closed channel bound - state calculations.
[c]Energy difference (eV) of the GRASP values with the NIST tabulations.
[d]MCDF ionization potential (eV) from Biemont and co-workers [38].
[e]Precentage difference of the GRASP values with the NIST tabulations.
[f]Precentage difference of the Breit-Pauli values with the NIST tabulations.
[†]Allowed transition to the ground state not considered in the present excited state cross section calculations.
[‡]Ionization potential (eV) determined from the present experiment was found to be 45.717 ± 0.030 eV.

experimental measurements. To simulate the ALS experimental measurements, a non-statistical averaging of the theoretical R-matrix photoionization cross-sections was performed for the ground and the metastable states which showed satisfactory agreement.

B. Hartee-Fock calculations

The Hartree-Fock approximation [44] assumes that each electron in the atom moves independently in the nuclear Coulomb field and the average field of the other electrons and so the N-electron wave function is just the anti-symmetrized product of N one-electron spatial wave functions. As a guide in the assignment of resonant features in the measurements, the Cowan atomic structure code [45], which is based on the relativistic Hartree-Fock (HFR) approximation, was used to calculate the energies and strengths of excitations contributing to the photoionization cross-section for K^{2+}. In the calculation of all transitions, $3s^23p^5$ was selected as the initial configuration. The final configurations selected were $3s^23p^4ns$ ($7 \leq n \leq 20$) for the $3p \rightarrow ns$ transitions, $3s^23p^4nd$ ($6 \leq n \leq 20$) for $3p \rightarrow nd$ transitions, and $3s3p^5np$ ($4 \leq n \leq 11$) for $3s \rightarrow np$ transitions.

IV. EXPERIMENTAL RESULTS AND ANALYSIS

A. Overview of measurements

An overview of the photoionization cross-section measurements over the photon energy range from 20 eV to 70 eV is presented in Fig. 1. The data from 20 eV to 44 eV were taken with an energy resolution of 0.1 eV, and those from 44 eV to 70 eV with a resolution of 0.045 eV. Vertical lines in the figure indicate the ionization threshold energies of the ground state (highest in energy) and different metastable states listed in Table I. Evidently long-lived metastable states constituted a significant fraction of the primary K^{2+} ion beam.

B. Ground-state ionization threshold

The ground-state configuration for the K^{2+} ion is $1s^22s^22p^63s^23p^5$, for which the Russell-Saunders notation gives the terms $^2P^o_{3/2}$ for the ground state and $^2P^o_{1/2}$ for the metastable state. Figure 2 shows the photoionization cross section for K^{2+} near the ground-state ionization threshold measured at a photon energy resolution of 0.004 eV. The ground-state ionization threshold was determined from the step to be 45.717 ± 0.030 eV. The measurement is 0.086 eV lower than the value tabulated in the NIST database [37] of 45.803 ± 0.012 eV which is the result from a multiconfiguration Dirac-Fock calculation [38]. Using the tabulated value of 0.268 eV for the fine-structure splitting [37] gives 45.449 eV for the ionization threshold of the $^2P^o_{1/2}$ metastable state.

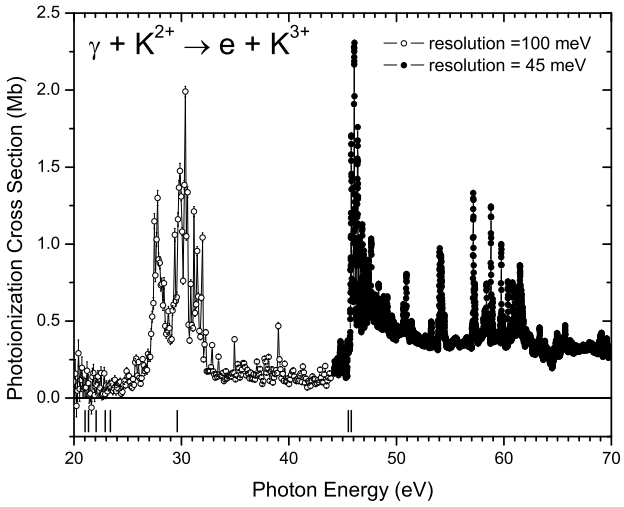

FIG. 1. Overview of photoionization cross-section measurements over the energy range 20–70 eV. The data from 20–44 eV (open circles) have an energy resolution of 0.1 eV and total uncertainty of ± 50%, while those from 44–70 eV (solid black circles) have a resolution of 0.045 eV and uncertainty of ± 22%. The vertical lines indicate the ionization threshold energies listed in Table I. The highest in energy is for the ground state and the remainder are for metastable states.

C. $3p \rightarrow nd$ transitions

Figure 3 shows the photoionization resonance structure in the energy range from below the ionization threshold of the $^2P^o_{1/2}$ metastable state to the $3s^23p^4(^1S)$ series limit of the K^{3+} ion. In this energy range eight Rydberg series due to $3p \rightarrow nd$ transitions differing in their final coupling between the excited electron and the core are characterized and assigned spectroscopically using the quantum defect form of the Rydberg formula. Of the eight series assigned in Figure 3, four converge to the $3s^23p^4(^1D_2)$ limit of K^{3+}, two originating from the $^2P^o_{1/2}$ metastable state and two from $^2P^o_{3/2}$ ground state. Transitions to the $3s^23p^4(^1D_2)nd(^2D^o)$ states (open diamonds) and $3s^23p^4(^1D_2)nd(^2P^o)$ (half bottom filled diamonds) states from the $^2P^o_{1/2}$ metastable state are not fully resolved. Only the lowest two members (n=9 and n=10) of the sequence are resolved from other Rydberg series. The corresponding series originating from the ground state are also not resolved from each other, only the lowest member (n=9) is resolved from other Rydberg series.

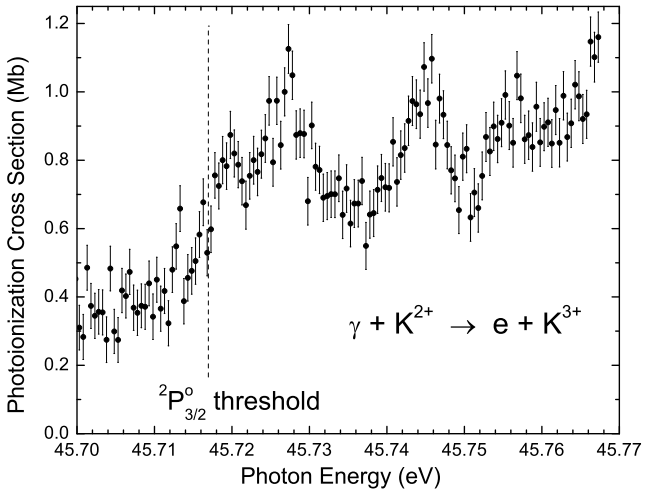

FIG. 2. Photoionization cross-section measurements at 0.004 eV resolution near the $^2P^o_{3/2}$ ground-state ionization threshold of K^{2+} at 45.717 eV.

The remaining four series converge to the $3s^23p^4(^1S_0)$ limit of K^{3+}. Two of these series originate from the $^2P^o_{1/2}$ metastable state and two from $^2P^o_{3/2}$ ground state. In the two series $3s^23p^5(^2P^o_{1/2}) \rightarrow 3s^23p^4(^1S)nd(^2D^o_{3/2})$ (open triangles) and $3s^23p^5(^2P^o_{1/2}) \rightarrow 3s^23p^4(^1S)nd(^2D^o_{5/2})$ (open inverted triangles), the first member (n=6) is not resolved from the other series, while the next three members (n=7, 8, 9) are resolved because their energy position is above the $3s^23p^4(^1D_2)$ limit. The situation is similar for the two corresponding series originating from the $3s^23p^5(^2P^o_{3/2})$ ground state.

The measured resonance energies, E_n (eV) of each of these series are plotted versus the principal quantum number n, in Figures A.1 and A.2 in Appendix A and fitted to the quantum defect form of the Rydberg formula [46],

$$E_n = E_\infty - \frac{\mathcal{Z}^2 Ry}{(n-\delta_n)^2}. \quad (1)$$

Here, n is the principal quantum number, δ_n the quantum defect, being zero for a pure hydrogenic state. The mean quantum defect is given by δ and the series limit E_∞ (eV) are free parameters where $\mathcal{Z} = Z - N_c$. The Rydberg constant (Ry = 13.6057 eV), nuclear charge (Z = 19) and the number of core electrons ($N_c = 16$) are fixed parameters. These eight Rydberg series are grouped together in Tables A.1 and A.2 in Appendix A by their energy positions, quantum defects δ_n, experimental series limits, and assignments. The tabulated series limits in the NIST database [37] for the $3s^23p^4(^1D_2)nd$ and $3s^23p^4(^1S_0)nd$ Rydberg series are 47.834 eV and 50.582 eV, respectively. A comparison of these limits with the experimental limits in Tables A.1 and A.2 provides additional evidence that the ground-state ionization threshold is 45.717 eV.

D. Additional metastable states

Below the ionization threshold of the $3s^23p^5(^2P^o_{1/2})$ metastable state at 45.450 eV, Figure 3 shows a non-zero photoionization cross section and small resonance features, suggesting population of more highly excited metastable states in the K^{2+} ion beam. Thus an overview energy scan at a photon energy resolution and energy step size of 0.1 eV was made down to 20 eV, shown in Figure 1. Strong resonance features are evident above 24.4 eV. Therefore photoionization measurements in the energy range 26 – 30 eV were made at a photon energy resolution of 0.045 eV and step size of 0.005 eV, as shown in Figure 5. The spectrum is dominated by a broad resonance feature of natural line width 1.15 eV, centered at 27.89 eV. This broad feature was initially speculated to be due to a $3s^23p^4(^3P_{2,1,0})n\ell$ dipole resonance originating from $3s^23p^4(^3P_{2,1,0})4s(^4P)$ metastable state. Narrow resonance features are superimposed upon the broad resonance. The non-zero cross section measured below the threshold of the $3s^23p^5(^2P^o_{1/2})$ metastable state is thus attributed to the presence of an undetermined fraction of the primary ion beam in the highly-excited $3s^23p^4(^3P)4s(^4P)$ metastable states, which have an ionization threshold of 19.93 eV [37].

For an initial estimate the fraction of the $3s^23p^4(^3P_{2,1,0})4s\ ^4P$ metastable states in the primary ion beam, the Cowan atomic structure code was used to calculate the direct photoionization cross sections from these states. The calculated direct photoionization cross section from $3s^23p^4(^3P_{2,1,0})4s\ ^4P_{5/2,3/2,1/2}$, $3s^23p^5(^2P^o_{3/2})$ and $3s^23p^5(^2P^o_{1/2})$ states near their ionization thresholds are 0.14 Mb, 0.37 Mb, and 0.12 Mb. Comparing these values to the measured non-resonant photoionization cross sections, approximately 25% of the primary K^{2+} ion beam is estimated to be in the $3s^23p^4(^3P_{2,1,0})4s\ ^4P$ metastable states, 25% in the $3s^23p^5(^2P^o_{1/2})$ metastable state and 50% in the $3s^23p^5(^2P^o_{3/2})$ ground state.

E. Inner-shell $3s \rightarrow np$ transitions

Figure 6 shows the photoionization resonance structure for K^{2+} in the photon energy range 50.149 – 69.741 eV where several series of resonances due to $3s \rightarrow np$ inner-shell excitations are visible. Three Rydberg series are assigned to excitation of the $3s3p^5(^3P^o_2)np$, $3s3p^5(^3P^o_1)np$ and $3s3p^5(^3P^o_0)np$ states from the $^2P^o_{1/2}$ metastable state, converging to the limits of 62.291 ± 0.034 eV, 62.378 ± 0.034 eV, and 62.705 ± 0.067 eV, respectively. The three corresponding series originating from the $^2P^o_{3/2}$ ground state converge to the limits of 62.356 ± 0.034 eV, 62.535

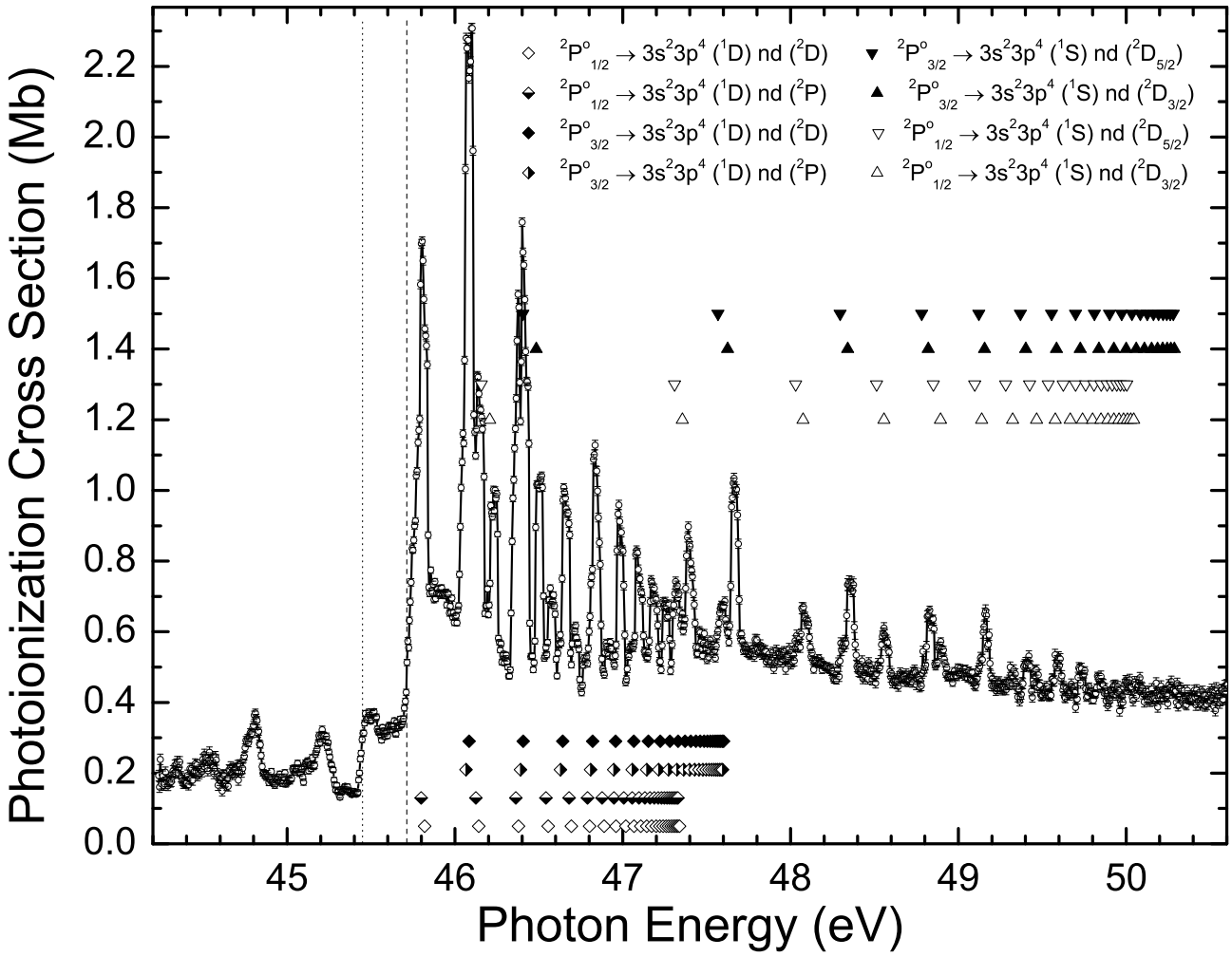

FIG. 3. Absolute cross-section measurements for photoionization of K^{2+} at a photon energy resolution of 0.045 eV. Vertical dashed and dotted lines indicate the $^2P^o_{3/2}$ ground-state and $^2P^o_{1/2}$ metastable-state ionization threshold energies. Eight Rydberg series of resonances from the $^2P^o_{1/2}$ metastable state and $^2P^o_{3/2}$ ground state of K^{2+} converging to the $3s^23p^4(^1D_2)$ and $3s^23p^4(^1S_0)$ limits of K^{3+} are identified. The measured cross section below the $^2P^o_{1/2}$ threshold is attributed to population of higher lying quartet metastable states in the K^{2+} ion beam.

$\pm$ 0.034 eV, and 62.547 $\pm$ 0.034 eV, respectively. A Rydberg series, $3s3p^5(^1P^o_1)np$, originating from the $^2P^o_{1/2}$ metastable state and converging to the series limit of 66.993 $\pm$ 0.049 eV, and a corresponding series originating from the $^2P^o_{3/2}$ ground-state and converging to the series limit of 67.017 $\pm$ 0.049 eV are also assigned in Figure 6. The measured resonances of the eight Rydberg series in Figure 6 are plotted versus the principal quantum number, n, as shown in Figure A.3 and fitted to the quantum defect form of the Rydberg formula [46] with mean quantum defect parameter δ and series limit E_∞ as free parameters. These series are grouped in Tables A.3, A.4, and A.5 by their measured energy positions, quantum defect parameters δ_n, series limits, and assignments. The tabulated series limits in the NIST database [37] for the series $3s3p^5(^3P^o_2)np$, $3s3p^5(^3P^o_1)np$, $3s3p^5(^3P^o_0)np$, and $3s3p^5(^1P^o_1)np$ are 62.440 eV, 62.623 eV, 62.721 eV, and 67.022 eV, respectively. A comparison of these limits with the experimental limits in Tables A.3, A.4, and A.5 provides additional evidence that the ground-state ionization threshold is 45.717 eV. An interesting question concerns the oscillator strengths of the assigned $3s3p^5(^3P^o_{2,1})4p$ and $3s3p^5(^3P^o_{2,1})5p$ resonances. It is assumed that for n values higher than 4, the $^2P^o_{3/2} \rightarrow 3s3p^5(^3P^o_2)np$ resonances and $^2P^o_{1/2} \rightarrow 3s3p^5(^3P^o_1)np$ resonances are unresolved from each other. Asymmetric Fano-Beutler resonance lineshapes [47] are evident in Figure 6 for the $3s \rightarrow np$ resonances. This is attributed to

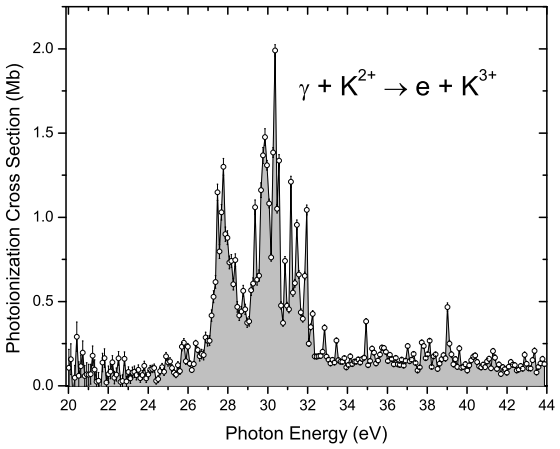

FIG. 4. Overview of photoionization cross-section measurements over the energy range 20 - 44 eV at a photon energy resolution of 0.1 eV and energy step size of 0.1 eV.

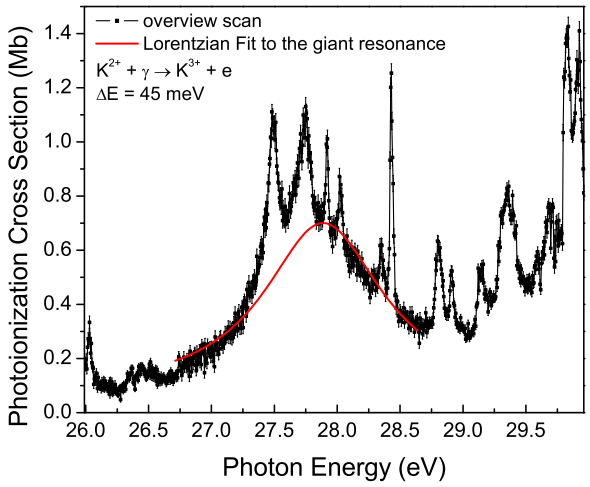
overview scan
Lorentzian Fit to the giant resonance
K2+ + γ → K3+ + e
ΔE = 45 meV
Photoionization Cross Section (Mb)
Photon Energy (eV)

FIG. 5. (Color online) Absolute photoionization cross-section measurements for K^{2+} at a photon energy resolution of 0.045 eV in the photon energy range 26 – 30 eV. The solid line represents a Lorentzian fit to the broad resonance feature attributed to photoionization from the $3d^4P_{5/2,3/2,1/2}$, $4s^4P_{5/2,3/2,1/2}$ and $3d^4G_{9/2,7/2}$ metastable states.

interference between the direct and the indirect photoionization channels for excitation of the $3s$ subshell.

V. COMPARISON WITH R-MATRIX THEORY

To further address the metastable content in the K^{2+} parent ion beam, semi-relativistic R-matrix calculations in intermediate coupling of cross sections for photoionization were carried out from the ground state and all the metastable states up to and including those from the $3s^23p^4(^3P)4s(^4P)$ levels. Table I lists all eighteen states investigated and the various excitation thresholds calculated from the semi-relativistic R-matrix approach compared to the available experimental data. Figures B.1 - B.5 in Appendix B present the cross section as a function of photon energy for these R-matrix calculations for the ground and the metastable levels that are listed in Table I. For all of the metastable states investigated up to and including those from the $3s^23p^4(^3P)4s(^4P)$ levels, the R-matrix cross section calculations indicate minimal presence of resonance features in the photon energy region 44 – 70 eV. However, resonances in the cross sections at photon energies below 44 eV are much stronger. In the photon energy range 26 – 30 eV one sees the main features are a broad shoulder resonance located at around 28 eV superimposed by peaks in the cross sections which are due to the presence of the $3d(^4P_{5/2,3/2,1/2})$, $4s(^4P_{5/2,3/2,1/2})$ and $3d(^2G_{7/2,9/2})$ metastable states in the K^{2+} primary ion beam.

A comparison in the photon energy range 44 – 70 eV between the present experiment and the semi-relativistic R-matrix intermediate-coupling cross-section calculations indicates best agreement with a non-statistical distribution among the 18 possible initial states listed in Table I. Assuming 25% population of the $3s^23p^5(^2P^o_{3/2})$ ground state and 25% in the $3s^23p^5(^2P^o_{1/2})$ metastable state gives best agreement between theory and experiment, with the remaining 50% distributed among the more highly excited metastable states listed in Table I. Figure 7 illustrates this comparison between the measurements and semi-relativistic intermediate coupling R-matrix results. The integrated oscillator strength f from the R-matrix calculations is 0.106, which compares favorably with the experimental value of 0.097 ± 0.021.

VI. SUMMARY AND CONCLUSIONS

Absolute photoionization cross-section measurements for K^{2+} were performed at fixed photon energy resolution of 0.045 eV in the photon energy range 44.24 – 69.74 eV. High-resolution measurements near the ground-state ionization threshold were performed at a photon energy resolution of 0.004 eV. The ground-state ionization threshold was determined to be 45.717 ± 0.030 eV, which is 0.089 eV lower than the value tabulated in the NIST database [37]. A non-zero photoionization cross section below the $3s^23p^5(^2P^o_{1/2})$ metastable state was observed that is attributed to ionization from higher-lying metastable states. The Cowan Hartree-Fock atomic structure code

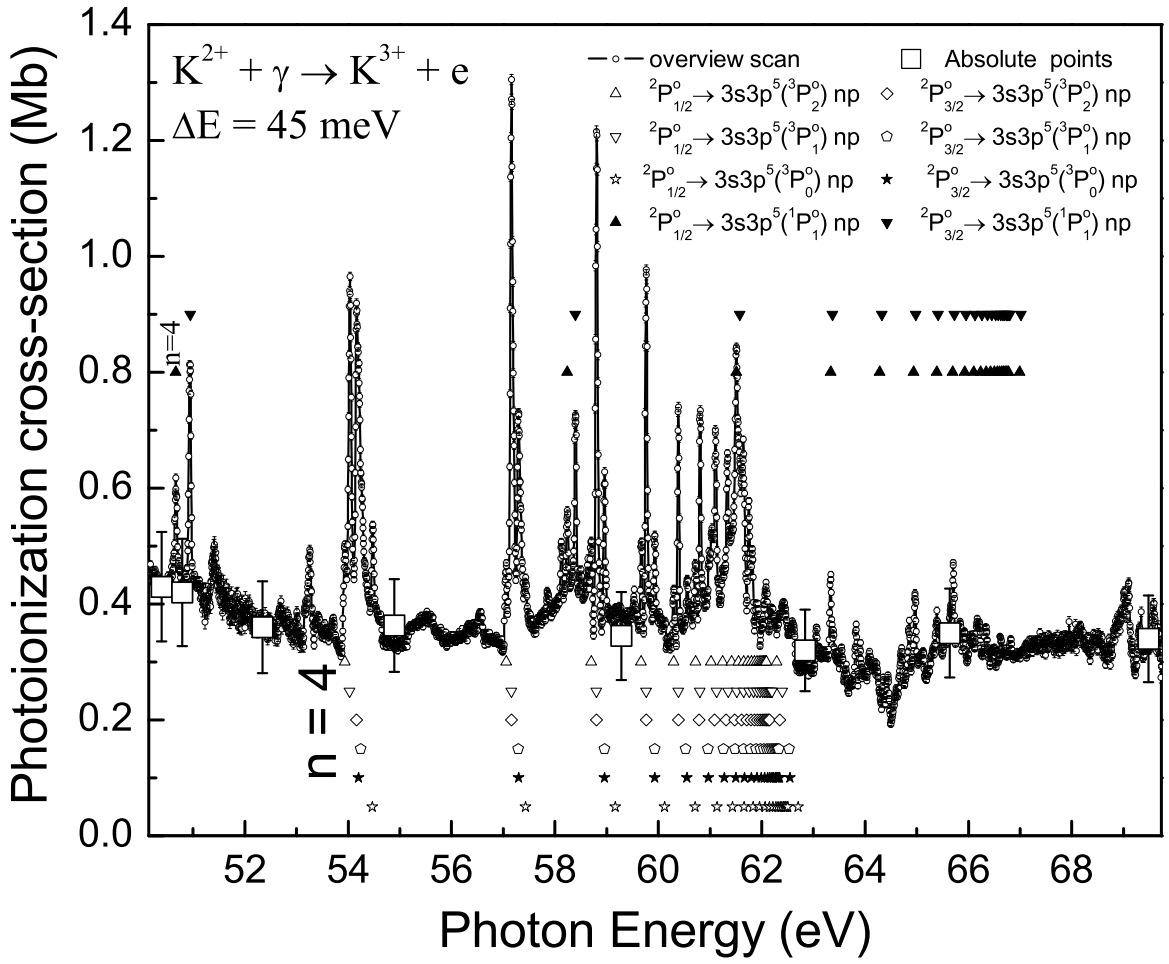

FIG. 6. Absolute photoionization cross-section measurements for K^{2+} at 0.045 eV resolution in the energy range from 51.4 eV to 69.7 eV. Open squares with error bars represent absolute measurements to which the energy scan is normalized. Eight Rydberg series of resonances due to inner-shell excitation $3s \rightarrow np$ converging to the $^3P^o_2$, $^3P^o_1$, $^3P^o_0$, and $^1P^o_1$ excited states of K^{3+} are identified.

was used to perform atomic-structure calculations to guide the assignments of the resonant features to Rydberg series. Eight Rydberg series of $3p \rightarrow nd$ resonances originating from both the $3s^2 3p^5(^2P^o_{1/2})$ metastable state and $3s^2 3p^5(^2P^o_{3/2})$ ground state were identified and spectroscopically assigned using the quantum defect theory. Eight more Rydberg series of resonances due to $3s \rightarrow np$ inner-shell excitations were also identified. These series (due to $3p \rightarrow nd$ and $3s \rightarrow np$ transitions) are tabulated according to their measured energy positions, quantum defect parameters, series limits, and assignments. The limits for the assigned Rydberg series provide additional evidence that the ground-state ionization potential of K^{2+} is 45.717 eV.

Detailed calculations using the Breit-Pauli approximations within the R-matrix approach were performed from the ground state and all metastable states lying below the $3s^2 3p^4(^3P)4s(^4P)$ levels over the photon energy range 20 – 70 eV. Suitable agreement with experiment is found with the intermediate coupling R-matrix calculations using a non-statistical initial distribution among the metastable and ground states of the system. The present semi-relativistic R-matrix calculations are consistent with 25% of the parent K^{2+} ion beam in the ground state, 25% in the $3s^2 3p^5(^2P^o_{1/2})$ metastable state the remaining 50% distributed among the high-lying

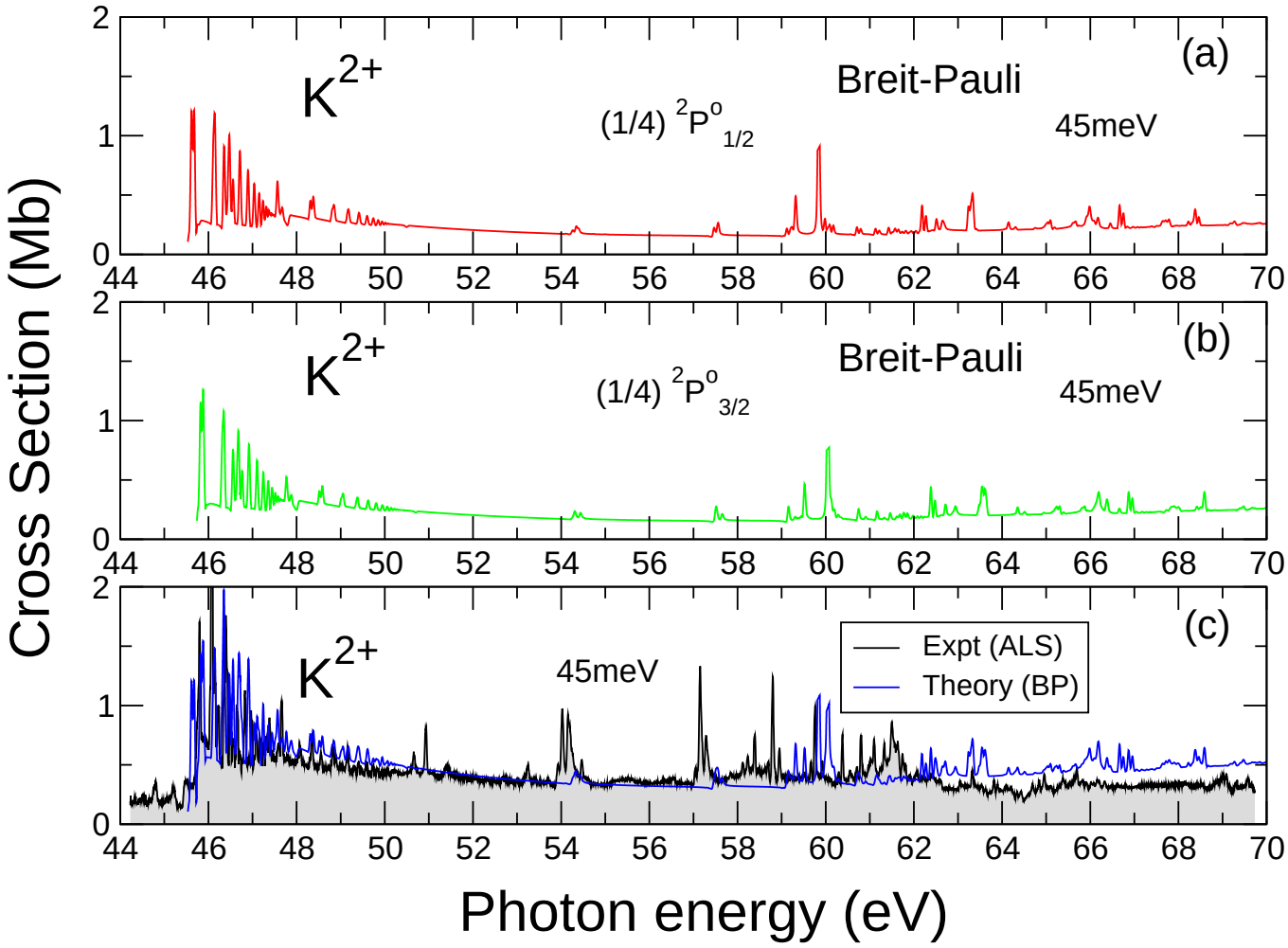

FIG. 7. Breit-Pauli R-matrix photoionization cross section calculations for the metastable (a)(1/4) $3s^2 3p^5\ ^2P^\circ_{1/2}$ and (b) $(1/4)3s^2 3p^5\ ^2P^\circ_{3/2}$ ground state of K^{2+} and (c) comparison between theory and experiment. The theoretical results has been convoluted with a Gaussian distribution having a profile of 45 meV FWHM to simulate the photon energy resolution of the experiment and a non-statistical admixture of the ground state and metastable states in the primary K^{2+} ion beam (see text for details).

metastable states considered for this system up to the $3s^2 3p^4(^3P)4s(^4P)$ levels.

The photoionization cross-sections from the present study are suitable for inclusion into state-of-the-art photoionization modeling codes such as CLOUDY [8, 9], XSTAR [48] and AtomDB [49] that are used to numerically simulate the thermal and ionization structure of ionized astrophysical nebulae.

ACKNOWLEDGMENTS

The Division of Chemical Sciences, Geosciences, and Biosciences of the U.S. Department of Energy supported this research under grant DE-FG02-03ER15424 and contract DE-AC03-76SF-00098. C. C. acknowledges support from PAPIT-UNAM IN107912-IN10261, Mexico. B. M. McL. acknowledges support by the U.S. National Science Foundation, under the visitors program, through a grant to ITAMP at the Harvard-Smithsonian Center for Astrophysics where this work was completed and a visiting research fellowship from Queen's University Belfast. The computational work was performed at the National Energy Research Scientific Computing Center in Oakland, CA, and on the Kraken XT5 facility at the National Institute for Computational Science (NICS) in Knoxville, TN. The Kraken XT5 facility is a resource of the Extreme Science and Engineering Discovery Environment (XSEDE), which is supported by National Science Foundation grant number OCI-1053575. The Advanced Light Source, is supported by the Director, Office of Science, Office of Basic Energy Sciences of the US Department of Energy under Contract DE-AC02-05CH11231.

[1] D. R. Flower, *Atoms in Astrophysics* (Plenum Press, New York, USA, 1983) pp. 289 – 323.
[2] I. Hofmann, Laser Part. Beams **8**, 527 (1990).
[3] R. W. P. McWhirter and H. P. Summers, *Applied Atomic Collision Physics: Volume 2* (Academic Press, New York, USA, 1983) pp. 55 – 111.
[4] J. B. West, J. Phys. B: At. Mol. Opt. Phys. **34**, R45 (2001).
[5] J. B. West, Radiat. Phys. Chem **70**, 274 (2004).
[6] H. Kjeldsen, J. Phys. B: At. Mol. Opt. Phys. **39**, R325 (2006).
[7] H. Feuchtgruber et. al., Astrophys. J. **487**, 962 (1997).
[8] G. Ferland, K. T. Korista, D. A. Verner, J. W. Ferguson, J. B. Kingdon, and E. M. Verner, Pub. Astron. Soc. Pac. (*PASP*) **110**, 761 (1998).
[9] G. J. Ferland, Ann. Rev. of Astron. & Astrophys. **41**, 517 (2003).
[10] P. R. Young, U. Feldman and A. Loebel, Astrophys. J. Suppl. Ser. **196**, 23 (2011).
[11] F. C. McKenna et al., Astrophys. J. Suppl. Ser. **109**, 225 (2000).
[12] S. Casassus, P. F. Roche and M. J. Roche, Mon. Not. R. Astron. Soc. **314**, 657 (2000).
[13] M. Martins, A. S. Schlachter, A. M. Covington, A. Aguilar, I. Alvarez, C. Cisneros, M. F. Gharaibeh, G Hinojosa, M. M. SantAnna, R. A. Phaneuf and B. M. McLaughlin, in *Thirteenth International VUV Conference* (Trieste, Italy, July 23-27, 2001).
[14] W. C. Stolte, Z. Felfli, R. Guillemin, G. Öhrwall, S.-W. Yu, J. A. Young, D. W. Lindle, T. W. Gorczyca, N. C. Deb, S. T. Manson, A. Hibbert, and A. Z. Msezane, Phys. Rev. A **88**, 053425 (2013).
[15] K. Kimura, T. Ymazaki, and Y. Achiba, Chem. Phys. Lett. **58**, 104 (1978).
[16] B. Ruščić and J. Berkowitz,, Phys. Rev. Lets. **50**, 675 (1983).
[17] P. van der Meulen, M. O. Krause, C. D. Caldwell, S. B. Whitfield, and C. A. de Lange, Phys. Rev. A **46**, 2468 (1992).
[18] M. O. Krause, C. D. Caldwell, S. B. Whitfield, C. A. de Lange, and P. van der Meulen, Phys. Rev. A **47**, 3015 (1993).
[19] G. A. AlnaWashi, M. Lu, M. Habibi, R. A. Phaneuf, A. L. D. Kilcoyne, A. S. Schlachter, C. Cisneros and B. M. McLaughlin, Phys. Rev. A **81**, 053416 (2010).
[20] A. M. Covington, A. Aguilar, I. Alvarez, C. Cisneros, I. R. Covington, I. Dominguez, M. F. Gharaibeh, G. Hinojosa, M. M. SantAnna, R. A. Phaneuf, and A. S. Schlachter, in *Proceedings of the XX11 International Conference on Photonic, Electronic and Atomic Collisions*, edited by S. Datz, M. E. Bannister, H. F. Krause, L. H. Saddiq, D. R. Schultz, and C. R. Vane (Rinton Press, Princeton, NJ, 2001) p. 48.
[21] A. M. Covington, A. Aguilar, I. R. Covington, G. Hinojosa, C. A. Shirley, R. A. Phaneuf, I. Alvarez, C. Cisneros, I. Dominguez-Lopez, M. M. SantAnna, A. S. Schlachter, C. P. Ballance, and B. M. McLaughlin, Phys. Rev. A **84**, 013413 (2011).
[22] F. Combet. Farnoux, M. Lamoureux, and K. T. Taylor, J. Phys. B: At. Mol. Phys. **11**, 2855 (1978).
[23] P. G. Burke and K. A. Berrington, *Atomic and Molecular Processes: An R-matrix Approach* (IOP Publishing, Bristol, UK, 1993).
[24] S. S. Tayal, Phys. Rev. A **47**, 182 (1993).
[25] Z. Felfli, N. C. Deb, D. S. F. Crothers, and A. Z. Msezane, J. Phys. B: At. Mol. Phys. **35**, L419 (2002).
[26] F. Robicheaux and C. H. Greene, Phys. Rev. A **46**, 3821 (1992).
[27] W. R. Fielder and L. Armstrong, Jr., Phys. Rev. A **28**, 218 (1983).
[28] M. Martins, J. Phys. B: At. Mol. Phys. **34**, 1321 (2001).
[29] J. A. R. Samson, Y. Shefer, and G. C. Angel, Phys. Rev. Letts. **56**, 2020 (1986).
[30] S. Shahabi, A. F. Starace, and T. N. Chang, Phys. Rev. A **30**, 1819 (1984).
[31] Z. D. Qian, S. L. Carter, and H. P. Kelly, Phys. Rev. A **33**, 1751 (1986).
[32] A. M. Covington, A. Aguilar, I. R. Covington, M. F. Gharaibeh, G. Hinojosa, C. A. Shirley, R. A. Phaneuf, I. Alvarez, C. Cisneros, I. Dominguez-Lopez, M. M. SantAnna, A. S. Schlachter, B. M. McLaughlin, and A. Dalgarno, Phys. Rev. A **66**, 062710 (2002).
[33] M. Lu, G. Alnawashi, M. Habibi, M. F. Gharaibeh, R. A. Phaneuf, A. L. D. Kilcoyne, E. Levenson, A. S. Schlachter, C. Cisneros, and G. Hinojosa, Phys. Rev. A **74**, 062701 (2006).
[34] P. G. Burke, *R-Matrix Theory of Atomic Collisions: Application to Atomic, Molecular and Optical Processes* (Springer, New York, USA, 2011).
[35] B. M. McLaughlin and C. P. Ballance, J. Phys. B: At. Mol. Opt. Phys. **45**, 095202 (2012).
[36] E. Biemont and J E Hansen, Phys. Scr. **34**, 116 (1986).
[37] Y. Ralchenko, A. E. Kramida, J. Reader, and N. A. Team, "NIST Atomic Spectra Database (version 4.0.1)," National Institute of Standards and Technology, Gaithersburg, MD, USA (2011).
[38] E. Biémont, Y. Frémat and P. Quinet, At. Data Nucl. Data Tables **71**, 117 (1999).
[39] J. E. Sansonetti, J. Phys. & Chem. Ref. Data **37**, 7 (2008).
[40] N. J. Wilson, A. Hibbert and K. L. Bell, Phys. Scr **61**, 603 (2000).
[41] K. G. Dyall, I. P. Grant, C. T. Johnson, and E. P. Plummer, Comput. Phys. Commun. **55**, 425 (1989).
[42] F. Parpia, C. F. Fischer, and I. P. Grant, Comput. Phys. Commun. **94**, 249 (2006).
[43] I. P. Grant, *Quantum Theory of Atoms and Molecules: Theory and Computation* (Springer, New York, USA, 2007).
[44] H. Friedrich, *Theoretical Atomic Physics,*, 2nd ed. (Springer, Berlin, Germany, 1981) pp. 85 – 92.
[45] R. D. Cowan, *The Theory of Atomic Structure and Spectra* (University of California Press, Berkeley, CA, USA, 1981).
[46] M. J. Seaton, Rep. Prog. Phys. **46**, 167 (1983).
[47] U. Fano and J. W. Cooper, Rev. Mod. Phys. **40**, 441 (1968).
[48] T. R. Kallman, Astrophys. J. Suppl. Ser. **134**, 139 (2001).
[49] A. R. Foster, L. Ji, R. K. Smith, and N. S. Brickhouse, Astrophys. J **756**, 128 (2012).

APPENDICES

A. Quantum-defect analyses of Rydberg series

B. R-Matrix theory results for the ground and metastable initial states

TABLE A.1. Principal quantum numbers n, resonance energies E_n (eV), series limit E_∞ (eV), and quantum defects δ_n of the $K^{2+}[3s^2 3p^4(^1D_2)]nd(^2P,\ ^2D)$ series estimated from the experimental measurements. Resonance energies are calibrated to within ±0.030 eV and the mean quantum defects δ have an estimated uncertainty of ±10%.

		Rydberg series $^1D_2$		Rydberg series
Initial state	n	E_n (eV)	δ_n	
$^2P^\circ_{1/2}$				
	[9d]	45.800	0.478 ± 0.064	
	10	46.118	0.539 ± 0.064	$[3s^2 3p^4(^1D_2)]nd(^2P)$
	11	46.381	0.475 ± 0.064	
	12	46.567	0.454 ± 0.064	
	.	.	.	
	∞	47.486 ± 0.038	δ = 0.527 ± 0.064	
$^2P^\circ_{1/2}$				
	[9d]	45.805	0.557 ± 0.062	
	10	46.133	0.612 ± 0.062	
	11	46.406	0.528 ± 0.062	$[3s^2 3p^4(^1D_2)]nd(^2D)$
	12	46.588	0.555 ± 0.062	
	.	.	.	
	∞	47.522 ± 0.038	δ = 0.601 ± 0.062	
$^2P^\circ_{3/2}$				
	[9d]	46.066	0.444 ± 0.037	
	10	46.375	0.523 ± 0.037	
	11	46.633	0.478 ± 0.037	
	12	46.810	0.520 ± 0.037	$[3s^2 3p^4(^1D_2)]nd(^2P)$
	13	46.966	0.411 ± 0.037	
	14	47.077	0.395 ± 0.037	
	15	47.163	0.415 ± 0.037	
	.	.	.	
	∞	47.739 ± 0.034	δ = 0.506 ± 0.037	
$^2P^\circ_{3/2}$				
	[9d]	46.073	0.451 ± 0.012	
	10	46.401	0.466 ± 0.012	
	11	46.648	0.448 ± 0.012	
	12	46.830	0.451 ± 0.012	$[3s^2 3p^4(^1D_2)]nd(^2D)$
	13	46.977	0.401 ± 0.012	
	14	47.083	0.435 ± 0.012	
	15	47.168	0.465 ± 0.012	
	.	.	.	
	∞	47.748 ± 0.034	δ = 0.488 ± 0.012	

TABLE A.2. Principal quantum numbers n, resonance energies E_n (eV), series limit E_∞ (eV), and quantum defects δ_n of the $K^{2+}[3s^2 3p^4(^1S_o)]nd(^2D_{3/2,5/2})$ series estimated from the experimental measurements. Resonance energies are calibrated to ±0.030 eV and the mean quantum defects δ are estimated with an uncertainty of ±10%.

		Rydberg series $^1S_0$		Rydberg series
Initial state	n	E_n (eV)	δ_n	
$^2P^\circ_{1/2}$				
	[6d]	46.229	0.481 ± 0.014	
	7	47.396	0.450 ± 0.014	
	8	48.093	0.466 ± 0.014	$[3s^2 3p^4(^1S_0)]nd(^2D_{3/2})$
	9	48.562	0.481 ± 0.014	
	10	48.901	0.473 ± 0.014	
	.	.	.	
	∞	50.249 ± 0.036	δ = 0.496 ± 0.014	
$^2P^\circ_{1/2}$				
	[6d]	46.188	0.481 ± 0.009	
	7	47.335	0.472 ± 0.009	
	8	48.037	0.491 ± 0.009	$[3s^2 3p^4(^1S_0)]nd(^2D_{5/2})$
	9	48.522	0.480 ± 0.009	
	10	48.870	0.436 ± 0.009	
	.	.	.	
	∞	50.209 ± 0.034	δ = 0.502 ± 0.009	
$^2P^\circ_{3/2}$				
	[6d]	46.507	0.469 ± 0.012	
	7	47.663	0.440 ± 0.012	
	8	48.355	0.460 ± 0.012	$[3s^2 3p^4(^1S_0)]nd(^2D_{3/2})$
	9	48.830	0.460 ± 0.012	
	10	49.163	0.461 ± 0.012	
	.	.	.	
	∞	50.509 ± 0.035	δ = 0.484 ± 0.012	
$^2P^\circ_{3/2}$				
	[6d]	46.431	0.504 ± 0.009	
	7	47.603	0.482 ± 0.009	
	8	48.310	0.498 ± 0.009	$[3s^2 3p^4(^1S_0)]nd(^2D_{5/2})$
	9	48.789	0.502 ± 0.009	
	10	49.133	0.483 ± 0.009	
	.	.	.	
	∞	50.485 ± 0.034	δ = 0.521 ± 0.009	

TABLE A.3. Principal quantum numbers n, resonance energies E_n (eV), series limit E_∞ (eV), and quantum defects δ_n of the $K^{2+}[3s^2 3p^5(^2P^o_{1/2}) \rightarrow 3s3p^5(^3P^o\ _{2,1,0})np]$ series estimated from the experimental measurements. Resonance energies are calibrated to ±0.030 eV and the mean quantum defects δ are estimated with an uncertainty of ±10%.

		Rydberg series $^3P_{2,1,0}$		Rydberg series
Initial state	n	E_n (eV)	δ_n	
$^2P^\circ_{1/2}$				
	[4p]	53.938	0.171 ± 0.002	
	5	57.061	0.161 ± 0.002	
	6	58.701	0.160 ± 0.002	$[3s3p^5(^3P^o_2)]np$
	7	59.671	0.165 ± 0.002	
	8	60.300	0.158 ± 0.002	
	9	60.715	0.186 ± 0.002	
	10	61.035	0.127 ± 0.002	
	11	61.255	0.130 ± 0.002	
	.	.	.	
	∞	62.291 ± 0.034	δ = 0.185 ± 0.002	
$^2P^\circ_{1/2}$				
	[4p]	54.032	0.171 ± 0.004	
	5	57.161	0.161 ± 0.004	
	6	58.806	0.160 ± 0.004	$[3s3p^5(^3P^o_1)]np$
	7	59.770	0.165 ± 0.004	
	8	60.390	0.158 ± 0.004	
	9	60.805	0.186 ± 0.004	
	10	61.105	0.127 ± 0.004	
	11	61.335	0.130 ± 0.004	
	.	.	.	
	∞	62.378 ± 0.034	δ = 0.181 ± 0.004	
$^2P^\circ_{1/2}$				
	[4p]	54.472	0.143 ± 0.023	
	5	57.431	0.181 ± 0.023	
	6	59.166	0.118 ± 0.023	$[3s3p^5(^3P^o_0)]np$
	7	60.125	0.110 ± 0.023	
	.	.	.	
	∞	62.705 ± 0.067	δ = 0.164 ± 0.023	

TABLE A.4. Principal quantum numbers n, resonance energies E_n (eV), series limit E_∞ (eV), and quantum defects δ_n of the $K^{2+}[3s^2 3p^5(^2P^o_{3/2}) \rightarrow 3s3p^5(^3P^o\ _{2,1,0})np]$ series estimated from the experimental measurements. Resonance energies are calibrated to ±0.030 eV and the mean quantum defects δ are estimated to within an error of 10%.

Initial state	n	Rydberg series $^3P_{2,1,0}$ E_n (eV)	δ_n	Rydberg series
$^2P^\circ_{3/2}$				
	[4p]	54.162	0.134 ± 0.004	
	5	57.161	0.145 ± 0.004	
	6	58.806	0.127 ± 0.004	$[3s3p^5(^3P^o_2)]np$
	7	59.770	0.119 ± 0.004	
	8	60.390	0.108 ± 0.004	
	9	60.805	0.115 ± 0.004	
	.	.	.	
	∞	62.356 ± 0.034	$\delta = 0.151 \pm 0.004$	
$^2P^\circ_{3/2}$				
	[4p]	54.242	0.157 ± 0.004	
	5	57.291	0.168 ± 0.004	
	6	58.961	0.147 ± 0.004	$[3s3p^5(^3P^o_1)]np$
	7	59.930	0.143 ± 0.004	
	8	60.555	0.135 ± 0.004	
	9	60.975	0.139 ± 0.004	
	.	.	.	
	∞	62.535 ± 0.034	$\delta = 0.174 \pm 0.004$	
$^2P^\circ_{3/2}$				
	[4p]	54.202	0.169 ± 0.002	
	5	57.301	0.168 ± 0.002	
	6	58.961	0.156 ± 0.002	$[3s3p^5(^3P^o_0)]np$
	7	59.930	0.159 ± 0.002	
	8	60.555	0.159 ± 0.002	
	.	.	.	
	∞	62.547 ± 0.034	$\delta = 0.184 \pm 0.002$	

TABLE A.5. Principal quantum numbers n, resonance energies E_n (eV), series limit E_∞ (eV), and quantum defects δ_n of the $K^{2+}[3s3p^5(^1P^o\ _1)]np$ series estimated from the experimental measurements. Resonance energies are calibrated to ±0.030 eV and the mean quantum defects δ are estimated to within an error of 10%.

		Rydberg series $^1P_1$		Rydberg series
Initial state	n	E_n (eV)	δ_n	
$^2P^\circ_{1/2}$				
	[4p]	50.664	1.262 ± 0.006	
	5	58.241	1.260 ± 0.006	$[3s3p^5(^1P^o_1)]np$
	6	61.510	1.275 ± 0.006	
	7	63.334	1.215 ± 0.006	
	.	.	.	
	∞	66.993 ± 0.049	δ = 1.272 ± 0.006	
$^2P^\circ_{3/2}$				
	[4p]	50.949	1.240 ± 0.006	
	5	58.396	1.231 ± 0.006	$[3s3p^5(^1P^o_1)]np$
	6	61.580	1.254 ± 0.006	
	7	63.374	1.202 ± 0.006	
	.	.	.	
	∞	67.017 ± 0.049	δ = 1.250 ± 0.006	

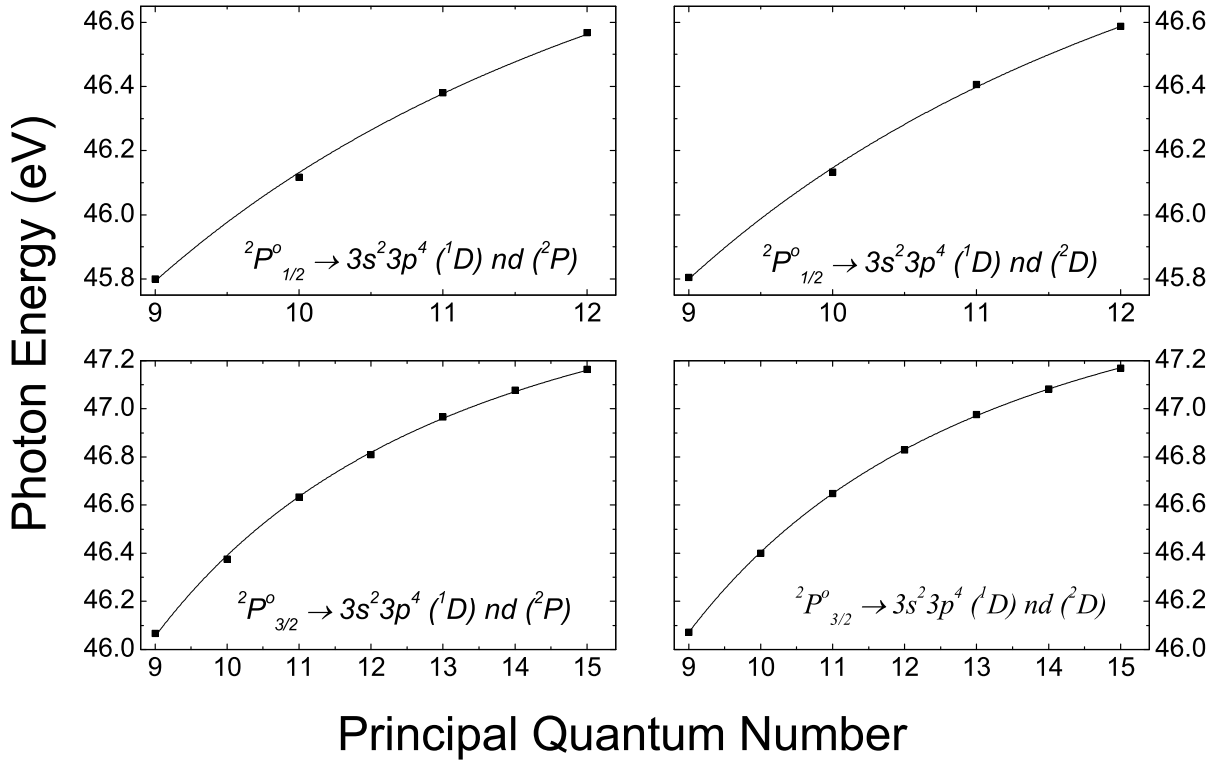
Photon Energy (eV)
Principal Quantum Number
$^2P^o_{1/2} \rightarrow 3s^2 3p^4\ (^1D)\ nd\ (^2P)$
$^2P^o_{1/2} \rightarrow 3s^2 3p^4\ (^1D)\ nd\ (^2D)$
$^2P^o_{3/2} \rightarrow 3s^2 3p^4\ (^1D)\ nd\ (^2P)$
$^2P^o_{3/2} \rightarrow 3s^2 3p^4\ (^1D)\ nd\ (^2D)$

FIG. A.1. Rydberg fits for the $3s^2 3p^4(^1D_2)nd$ series originating from both the $^2P^o_{3/2}$ ground state and the $^2P^o_{1/2}$ metastable state.

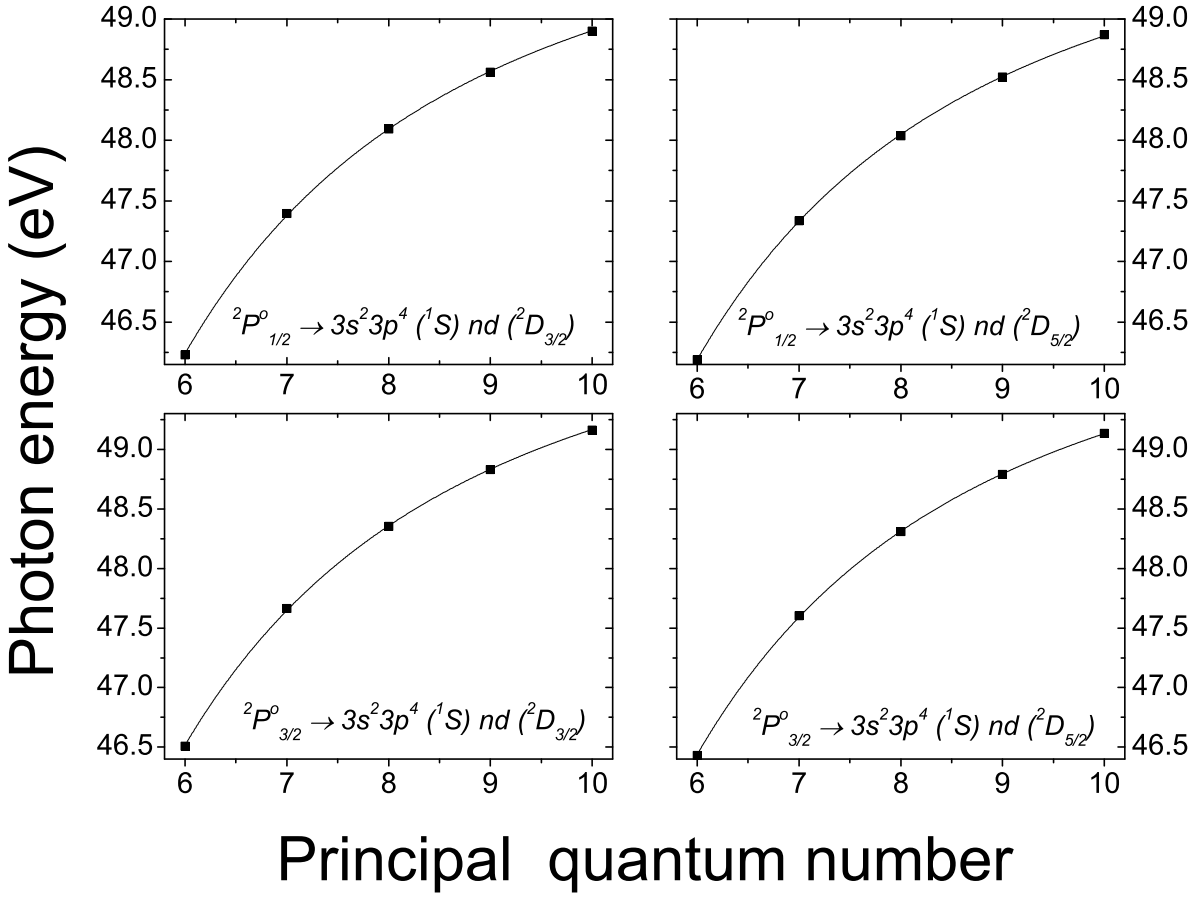
Photon energy (eV)
Principal quantum number
$^2P^o_{1/2} \rightarrow 3s^2 3p^4\ (^1S)\ nd\ (^2D_{3/2})$
$^2P^o_{1/2} \rightarrow 3s^2 3p^4\ (^1S)\ nd\ (^2D_{5/2})$
$^2P^o_{3/2} \rightarrow 3s^2 3p^4\ (^1S)\ nd\ (^2D_{3/2})$
$^2P^o_{3/2} \rightarrow 3s^2 3p^4\ (^1S)\ nd\ (^2D_{5/2})$

FIG. A.2. Fits of the Rydberg formula for the $3s^2 3p^4(^1S_0)nd$ resonance energies for series originating from the $^2P^o_{3/2}$ ground state and the $^2P^o_{1/2}$ metastable state.

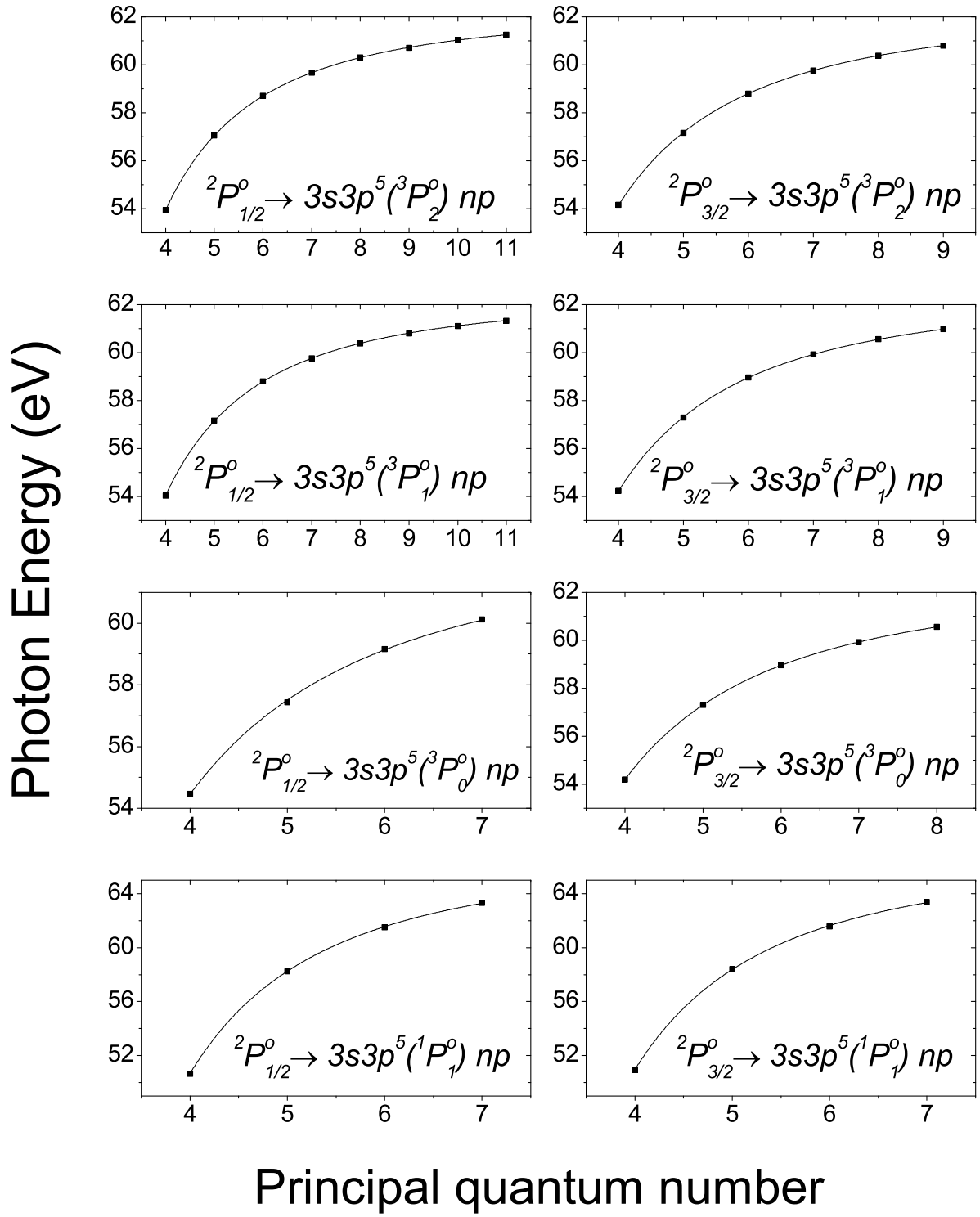

FIG. A.3. Fits of Rydberg formula for the $3s3p^5(^3P^o\ _{2,1,0})np$ and $3s3p^5(^1P^o\ _1)np$ series originating from the $^2P^o_{3/2}$ ground state and the $^2P^o_{1/2}$ metastable state.

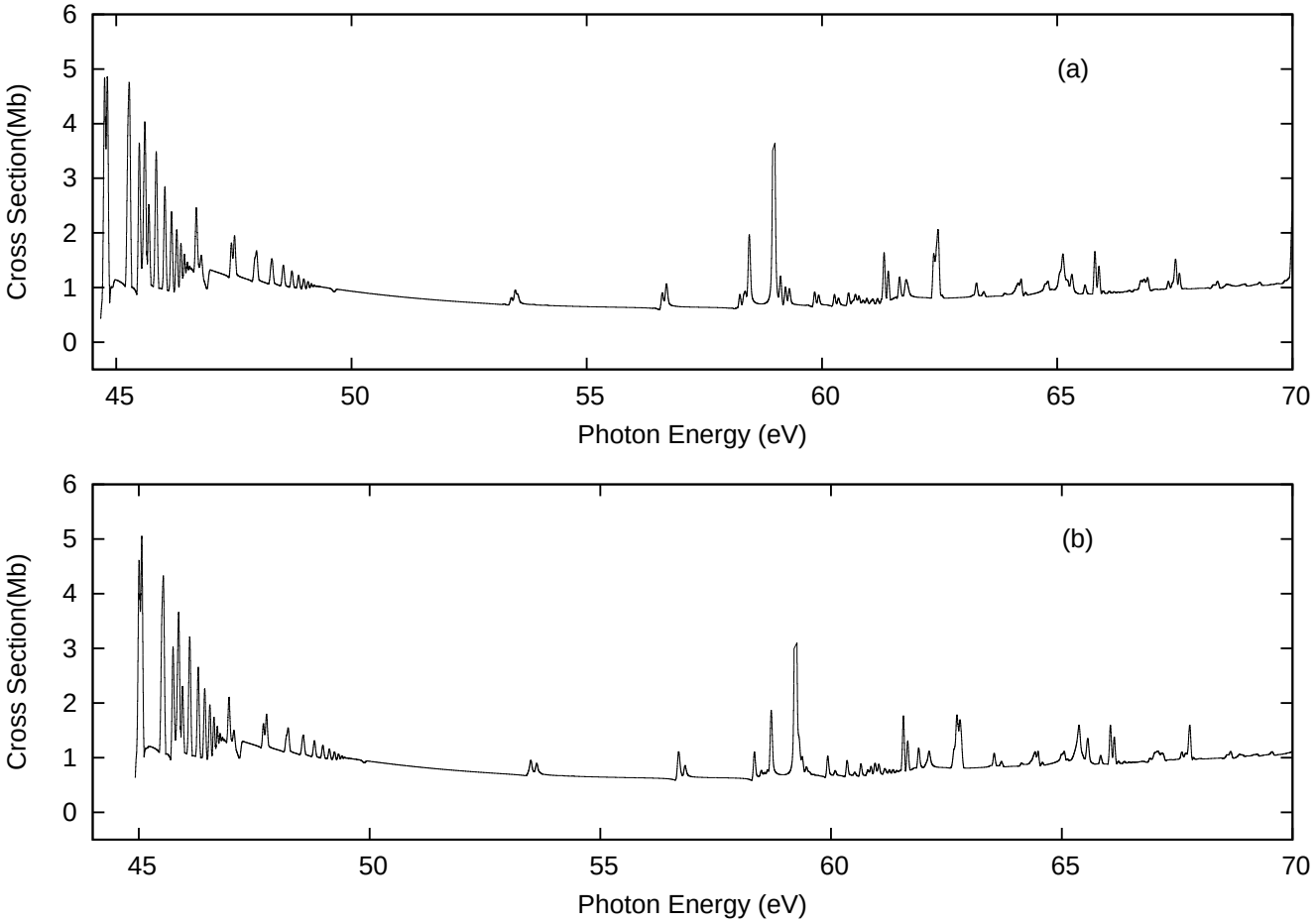

FIG. B.1. Breit-Pauli R-matrix photoionization cross section calculations for the metastable (a) $3s^2 3p^5\ {}^2P^\circ_{1/2}$ and (b) $3s^2 3p^5\ {}^2P^\circ_{3/2}$ ground state of K^{2+}. The theoretical results has been convoluted with a Gaussian of 45 meV FWHM to simulate the photon energy resolution of the experiment.

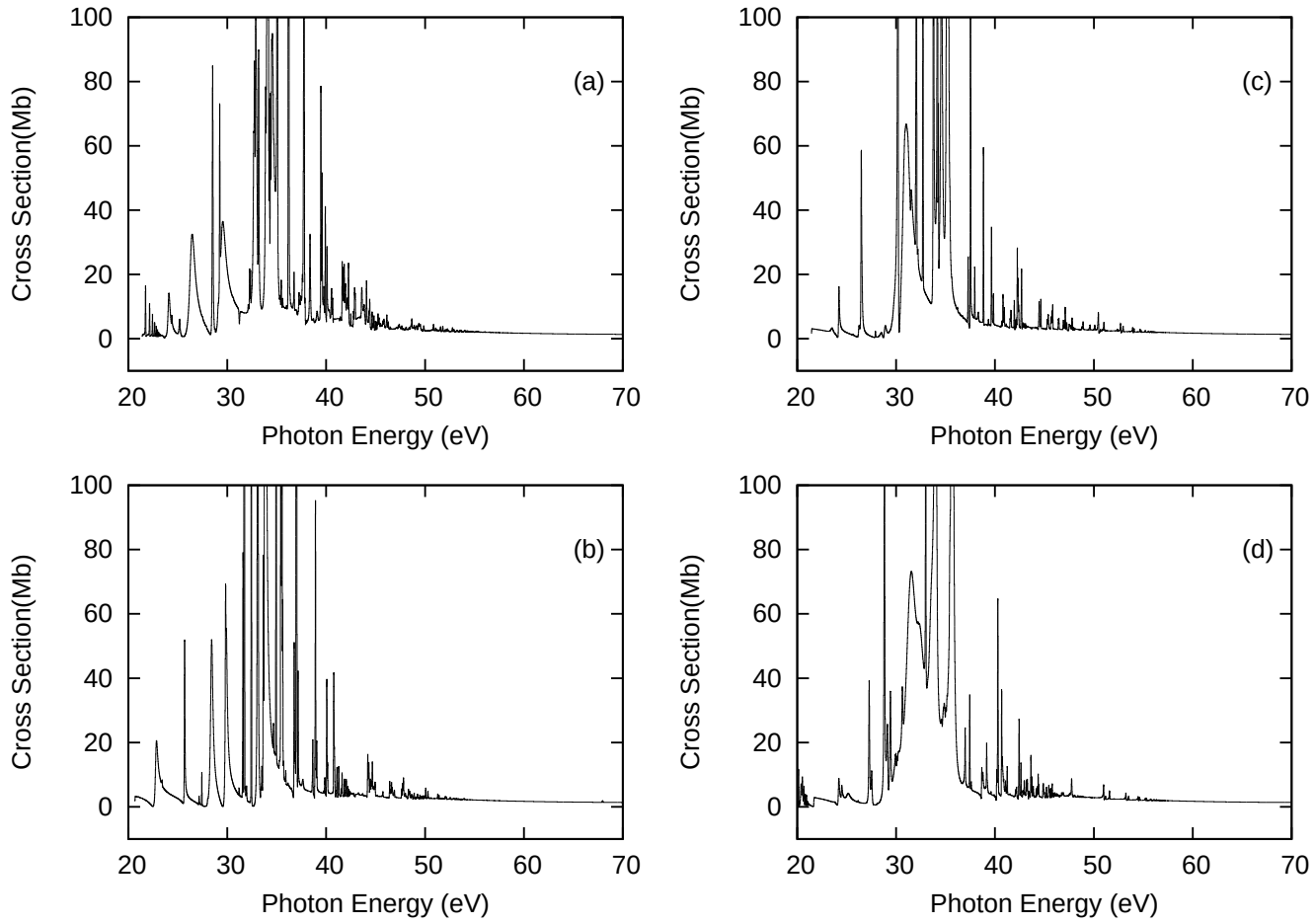

FIG. B.2. Breit-Pauli R-matrix photoionization cross section calculations for the (a) $3d\ ^4P_{1/2}$ and (b) $4s\ ^4P_{1/2}$, (c) $3d\ ^4F_{9/2}$ and (d) $3d\ ^2G_{9/2}$ metastable states of K^{2+} as listed in Table I. The theoretical results has been convoluted with a Gaussian of 45 meV FWHM to simulate the photon energy resolution of the experiment.

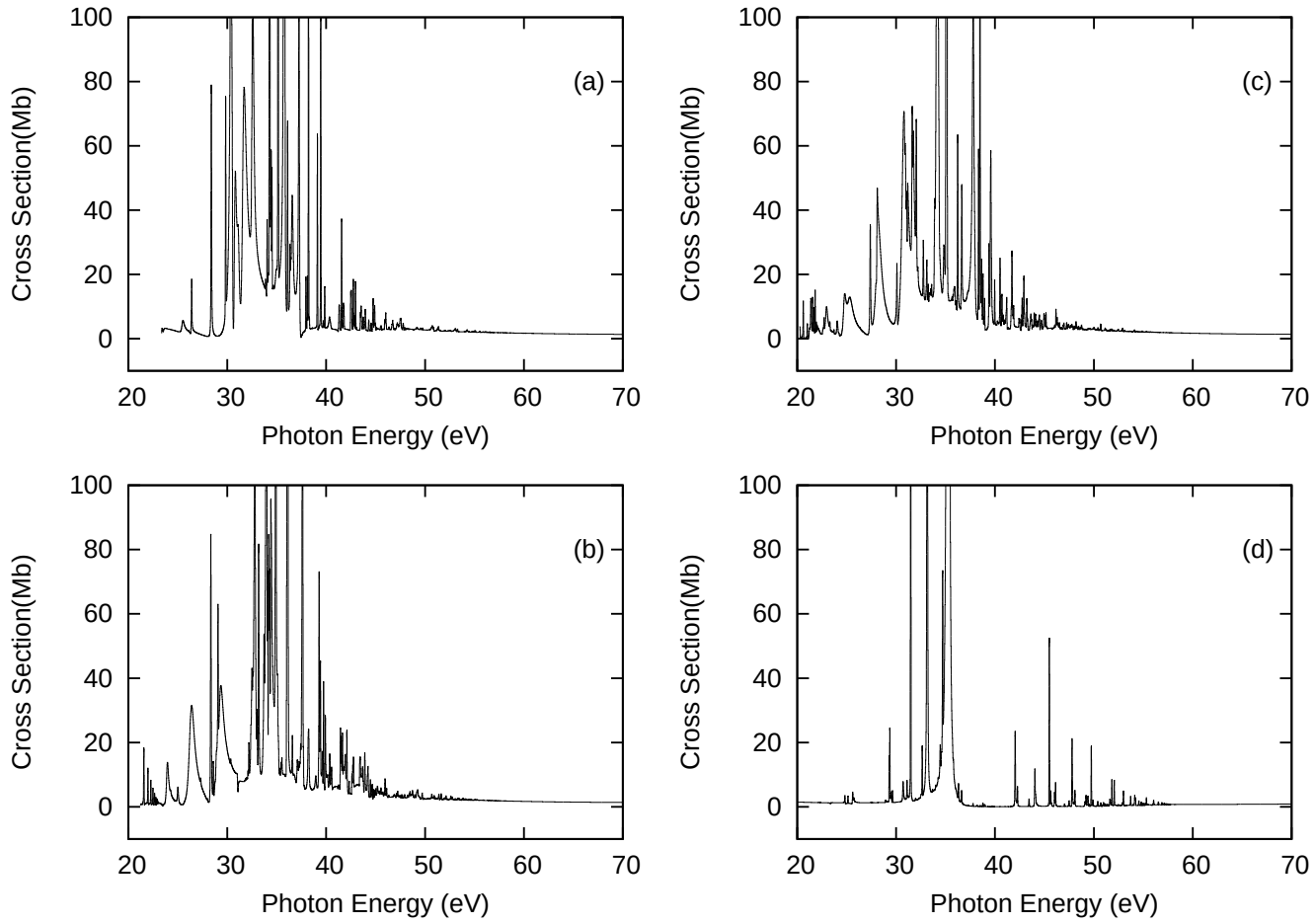

FIG. B.3. Breit-Pauli R-matrix photoionization cross section calculations for the (a) $3d\ ^4D_{3/2}$, (b) $3d\ ^4P_{3/2}$ (c) $4s\ ^4P_{3/2}$ and (d) $4s\ ^4P_{5/2}$ metastable states of K^{2+} as listed in Table I. The theoretical results has been convoluted with a Gaussian of 45 meV FWHM to simulate the photon energy resolution of the experiment.

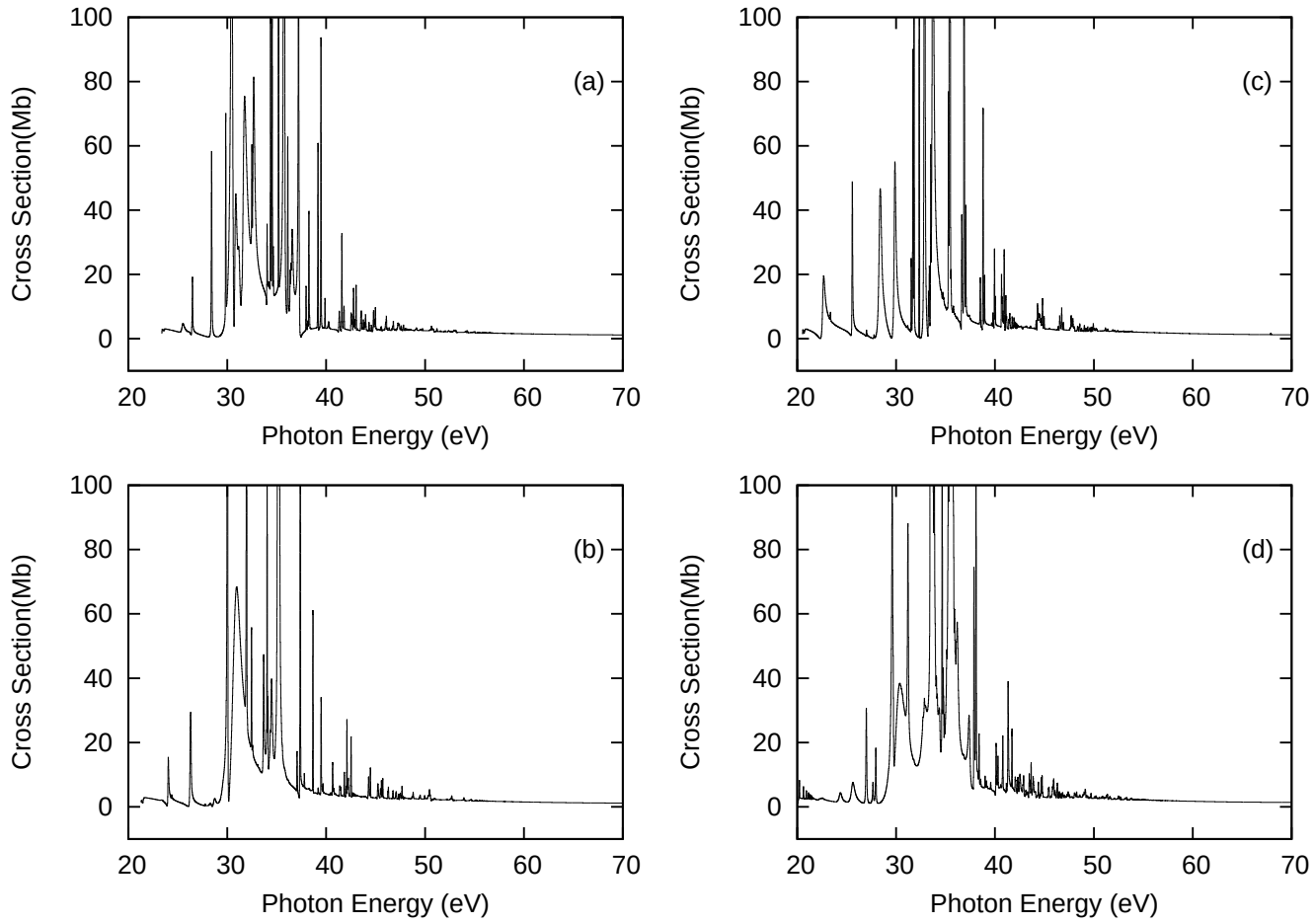

FIG. B.4. Breit-Pauli R-matrix photoionization cross section calculations for the (a) $3d\ ^4D_{5/2}$, (b) $3d\ ^4F_{5/2}$, (c) $3d\ ^4P_{5/2}$ and (d) $3d\ ^2F_{5/2}$ metastable states of K^{2+} as listed in Table I. The theoretical results has been convoluted with a Gaussian of 45 meV FWHM to simulate the photon energy resolution of the experiment.

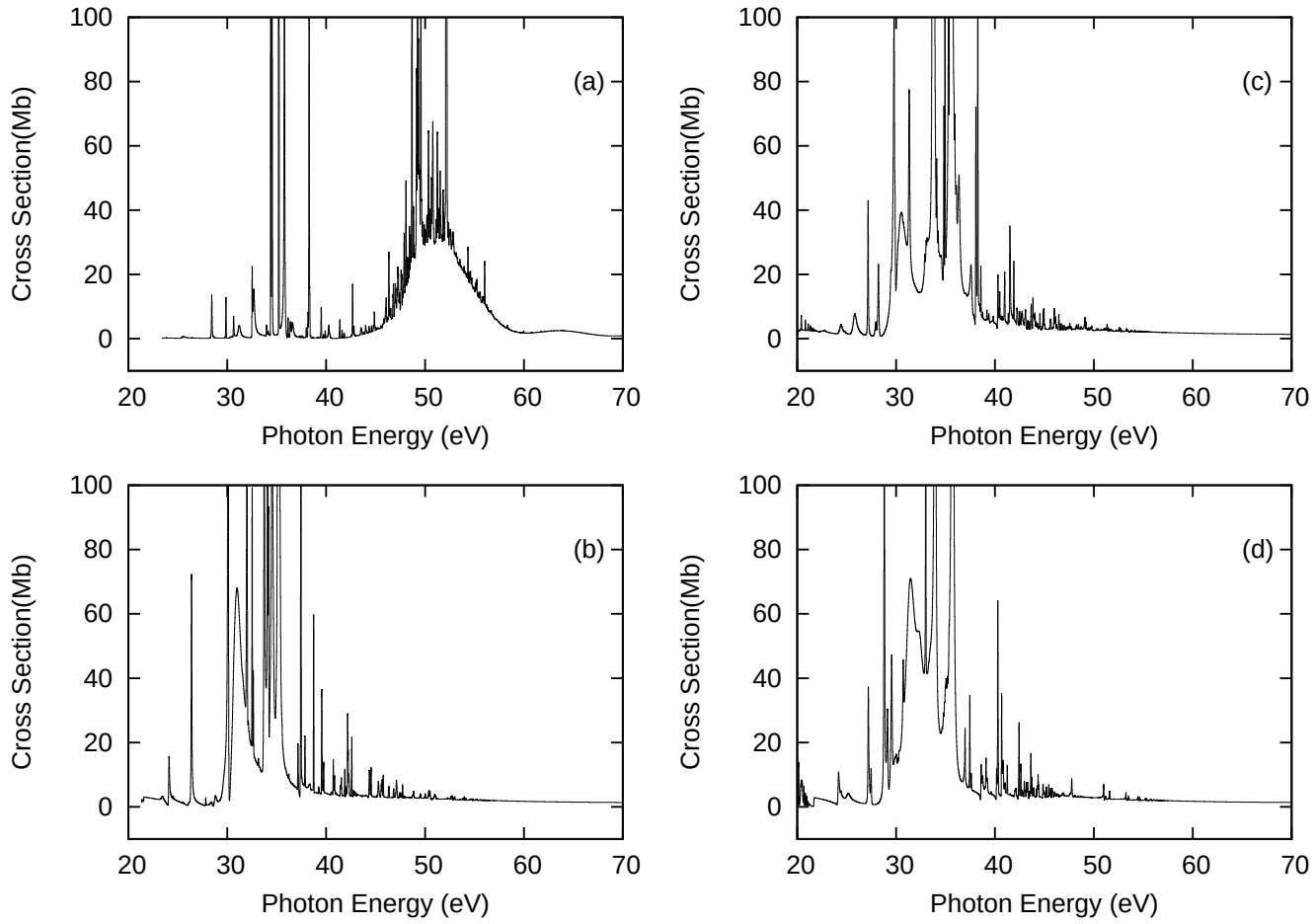

FIG. B.5. Breit-Pauli R-matrix photoionization cross section calculations for the (a) $3d\ ^4D_{7/2}$, (b) $3d\ ^4F_{7/2}$, (c) $3d\ ^2F_{7/2}$ and (d) $3d\ ^2G_{7/2}$ metastable states of K^{2+} as listed in Table I. The theoretical results has been convoluted with a Gaussian of 45 meV FWHM to simulate the photon energy resolution of the experiment.